Transport through (Ga,Mn)As nanoislands: Coulomb blockade and temperature dependence of the conductance

Markus Schlapps,[1] Teresa Lermer,[1] Stefan Geissler,[1] Daniel Neumaier,[1] Janusz Sadowski,[2,3] Dieter Schuh,[1] Werner Wegscheider,[1,4] and Dieter Weiss[1]

[1]*Institut für Experimentelle und Angewandte Physik, Universität Regensburg, 93040 Regensburg, Germany*
[2]*Max-Lab, Lund University, SE-223 63 Lund, Sweden*
[3]*Institute of Physics, Polish Academy of Sciences, 02-668 Warsaw, Poland*
[4]*Laboratory for Solid State Physics, 8093 Zurich, Switzerland*

(Received 20 April 2009; revised manuscript received 26 July 2009; published 25 September 2009)

We report on magnetotransport measurements of nanoconstricted (Ga,Mn)As devices showing very large resistance changes that can be controlled by both an electric and a magnetic field. Based on the bias voltage and temperature-dependent measurements down to the millikelvin range we compare the models currently used to describe transport through (Ga,Mn)As nanoconstrictions. We provide an explanation for the observed spin-valvelike behavior during a magnetic field sweep by means of the magnetization configurations in the device. Furthermore, we prove that Coulomb blockade plays a decisive role for the transport mechanism and show that modeling the constriction as a granular metal describes the temperature and bias dependence of the conductance correctly and allows to estimate the number of participating islands located in the constriction.

DOI: 10.1103/PhysRevB.80.125330 PACS number(s): 75.50.Pp, 73.23.Hk, 73.63.Rt, 85.75.Mm

I. INTRODUCTION

Narrow constrictions in thin stripes of the ferromagnetic semiconductor (Ga,Mn)As display interesting and huge magnetoresistance (MR) effects,[1–6] applicable, e.g., for sensors or nonvolatile memory elements.[5] The underlying mechanism causing these MR effects is still not unambiguously resolved. Initially it was believed that collinear alignment of the magnetization on both sides of the narrow together with a tunnel barrier, formed by side-wall depletion in the constriction, gives rise to a tunneling magnetoresistance effect (TMR).[1] In these experiments the in-plane magnetic field was aligned along the axis of the stripes. After the finding that the resistance as a function of direction and strength of an in-plane magnetic field is reminiscent of the anisotropic magnetoresistance (AMR), the observed MR effects were ascribed to a tunneling anisotropic magnetoresistance effect (TAMR),[2] originally observed in an $Au/AlO_x/(Ga,Mn)As$ sandwich structure.[7] There, the angular dependence arises from spin-orbit coupling which results in a magnetization-dependent density of states (DOS).[2] However, in the case of lateral structures, the variation in the DOS is ~50% (Ref. 2) and much too small to explain the MR effects, orders-of-magnitude larger.[3,4] A possible explanation was based on the assumption that a metal-insulator transition (MIT) occurs,[5,8] again driven by spin-orbit interaction and a magnetization-dependent overlap of hole wave functions. On the other hand, experiments on a narrow (Ga,Mn)As channel revealed a Coulomb blockade anisotropic magnetoresistance effect (CBAMR), where the angular dependence of the resistance is ascribed to chemical-potential anisotropies.[6] Here we revisit the problem of transport across a (Ga,Mn)As nanoconstriction. In order to shed light on the underlying transport mechanism, the bias, temperature, and gate dependence of the conductance is in the focus of the present paper. After a phenomenological explanation for the large MR effects and the evidence of Coulomb blockade (CB) we regard the constricted region as a granular metal and resort to a theoretical model to fit the measured bias and temperature dependence of the conductance.

II. SAMPLE FABRICATION AND MEASUREMENT SETUP

We fabricated samples with an individual nanoconstriction; an electron micrograph of the central region of one of the devices is shown in Fig. 1(a). The device consists of a 20-nm-thick $Ga_{0.95}Mn_{0.05}As$ film grown at 243 °C by low-temperature (LT) molecular-beam epitaxy on top of 5 nm $Al_{0.7}Ga_{0.3}As$, 3 nm LT GaAs, and a (001)-GaAs substrate. After annealing the unpatterned sample at 200 °C for 8.5 h the Curie temperature, determined from the temperature dependence of the resistance,[9] reached approximately 90 K at a carrier density of about 1.8×10^{20} cm^{-3}. The central area including the gates were defined by electron-beam lithography where cross-linked poly-methyl-methacrylate formed the etch mask. Chemically assisted ion-beam etching was then used to define the (Ga,Mn)As structure. Ti/Au contacts [not shown in Fig. 1(a)] were deposited as source-drain and gate electrodes. Each of the devices consists of a 3-μm-long and 700-nm-wide lead separated by a ~20 nm wide constriction from a 3-μm-long and 100-nm-wide lead. The structure is aligned along the [100] direction, that is, close to an easy axis of our (Ga,Mn)As films. Apart from that, strain relaxation in the stripes turns the easy axis toward the leads.[10] To determine the switching fields for a magnetization reversal in the wide and narrow stripes via the negative and anisotropic magnetoresistance effect some of the devices have additional potential probes on each stripe. Below we present data of two samples A and B. While sample A has no side gate, sample B has additional side electrodes [as presented in Fig. 1(a)], separated by ~130 nm from the constriction, to tune the electrostatic potential in the constriction. Magnetotransport measurements were carried out in a ^4He bath cryostat or a $^3He/^4He$ dilution refrigerator, each equipped with a superconducting magnet. The angle α between the applied in-plane magnetic field and the current direction could be varied

 ©2009 The American Physical Society

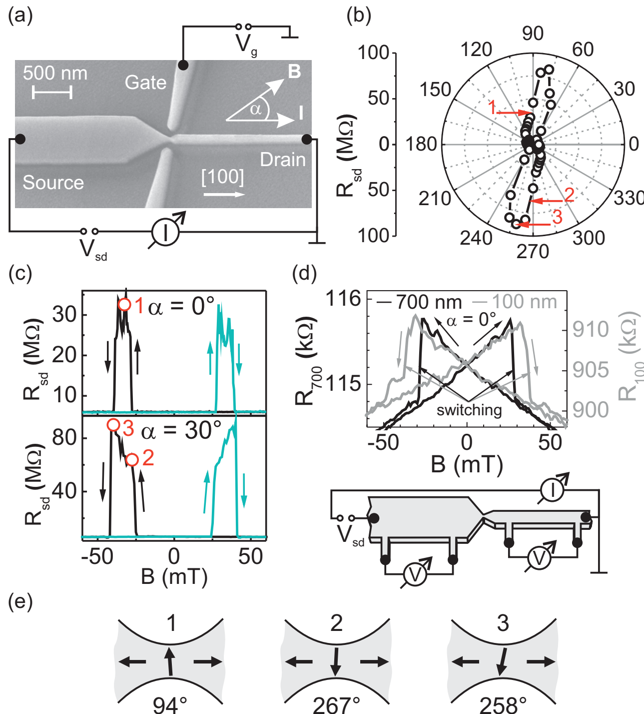

FIG. 1. (Color) (a) Electron micrograph of the central part of a device, tilted by 40°. (b) Polar plot of R_{sd} at 1.6 K showing the strong anisotropy of R_{sd} for sample A as a function of the magnetization direction. The measurement was done in a high magnetic field of 300 mT. (c) MR of sample A for $\alpha=0°$ and $\alpha=30°$ at 1.6 K. The switching fields of ±28 and ±38 mT (for $\alpha=0°$) correspond to the magnetization reversal of the broad and narrow lead, respectively. (d) Magnetization switching of the 700-nm-wide and 100-nm-wide stripe measured at 1.6 K for $\alpha=0°$ on a reference sample with additional voltage leads as shown in the sketch. Comparing the resistance values of (b) and (c) allows to deduce the magnetization alignment in the constriction. The configurations for a HR state together with the magnetization angle in the constriction is sketched in (e).

by rotating the sample inside the cryostat. The measurements were done using dc technique in a two-point configuration: a constant voltage V_{sd} between source and drain was applied and the resulting current I was measured employing a current amplifier.

III. PHENOMENOLOGICAL INTERPRETATION OF THE MR EFFECTS

First we demonstrate that the MR effects observed in our (Ga,Mn)As nanoconstrictions can be phenomenologically ascribed to the magnetization alignment in the narrow. Figure 1(b) shows a polar plot of the resistance R_{sd} of sample A measured at 1.6 K by rotating the sample in an in-plane magnetic field of 300 mT. This field strength is large enough to align all magnetization vectors into the external field direction. R_{sd} is strongly anisotropic with resistance changes in up to a factor of 20. Neither AMR, which in bulk (Ga,Mn)As is on the order of a few percent, nor TMR (magnetization in the leads is always parallel) or TAMR (change in DOS too small) can explain such drastic resistance changes.[4] Figure 1(c) displays the MR as a function of the in-plane field during a magnetic field sweep along the [100]-structure axis ($\alpha=0°$) and for the direction causing the largest MR effect ($\alpha=30°$). The switching fields of the spin-valvelike signal agree perfectly with the magnetization reversal fields of the 700-nm-wide and 100-nm-wide stripe that have been detected simultaneously by a four-point measurement using a reference sample with additional voltage probes on each lead. The magnetoresistance traces of the corresponding reference sample are shown in Fig. 1(d). Note that the switching fields are different due to a different strain relaxation.[10] The abrupt resistance changes stem from magnetization reversal in the respective stripe. The large resistance change in Fig. 1(c) can therefore be ascribed to the consecutive magnetization reversal of the 700 and the 100 nm stripe. The maximum resistance observed in the high-field experiment of Fig. 1(b) is in good agreement with the high resistance (HR) measured in the experiment of Fig. 1(c). This suggests that both effects stem from the same origin and that R_{sd} is linked to the magnetization direction in the constriction. Thus, by comparing the resistances of the polar plot of Fig. 1(b) with the spin-valvelike signal observed during a magnetic field sweep we can deduce the magnetization direction in the constriction and explain the MR trace by means of the magnetization alignments in the device. The magnetization configurations for the HR states marked with open circles in Fig. 1(c) are sketched in Fig. 1(e). So, at low external magnetic fields, the relative alignment of the magnetization in the wide and narrow stripe involves a distinct magnetization orientation in the constriction and thus determines the resistance. Within this picture the MR is easily explainable for an applied magnetic field along the stripe axis (i.e., $\alpha=0°$). Here, the HR state occurs due to the 180° magnetization reversal in the 700 nm stripe at -28 mT whereas the magnetization in the 100 nm stripe still remains in the [100] easy axis [see sketch 1 in Fig. 1(e)] until its coercive field is reached at -38 mT. It is important to note that it is not the antiparallel alignment of the stripes which, e.g., via the TMR effect, causes the HR state but the associated oblique orientation of the magnetization in the constriction. Also more complex features of the MR trace that appear for magnetic field angles $\alpha\neq0°$ can be understood. Consider, e.g., the MR in the case of $\alpha=30°$, shown in Fig. 1(c). The resistance increase within the magnetic field range marked with 2 and 3 arises from a coherent magnetization rotation in the constriction due to an increasing magnetic field strength along the $210°(\triangleq-30°)$ direction. This is illustrated schematically in the cartoons 2 and 3 of Fig. 1(e). The magnetizations in the leads remain unchanged in the considered magnetic field window due to the strong uniaxial anisotropy of the stripes. Increasing the magnetic field strength further leads to an abrupt 180° magnetization reversal in the 100 nm stripe causing the abrupt resistance change due to the resulting magnetization alignment in the constriction toward 180°.

IV. COULOMB BLOCKADE AS MICROSCOPIC ORIGIN OF THE MR EFFECTS

We now address the microscopic origin of the large MR effects and discuss the results with respect to the available

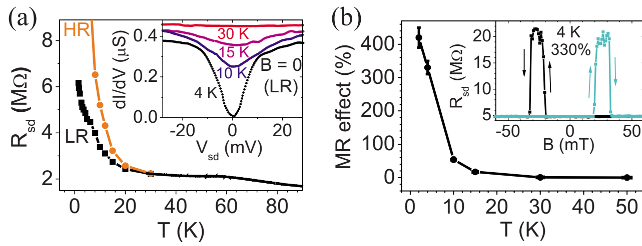

FIG. 2. (Color online) (a) Temperature dependence of R_{sd} for the low and high resistance state of sample A at $V_{sd}=15$ mV. The inset displays the differential conductance versus V_{sd} for different temperatures at $B=0$ showing insulating behavior below 30 K. (b) Temperature dependence of the MR effect observed during a magnetic field sweep at $V_{sd}=15$ mV. A corresponding MR measurement is shown for 4 K in the inset.

models, magnetization-induced MIT,[5] and Coulomb blockade.[6] At temperatures below $T\sim 30$ K the resistance of our patterned sample A increases continuously with decreasing temperature, both for the HR and low resistance (LR) state, see Fig. 2(a). The inset of Fig. 2(a) demonstrates that the *I-V* characteristic gets nonlinear below 30 K. Since the *I-V* curves were recorded at zero magnetic field, corresponding to a low resistance state, we conclude that our sample is fully in the insulating regime for $T<30$ K. The enhanced MR effects, on the other side, vanish above $\sim$30 K and thus only exist in the insulating regime. In Fig. 2(b) the size of the MR effects, taken from magnetic field sweeps like the one displayed in the inset of Fig. 2(b), is plotted versus temperature. A picture involving a magnetization driven MIT, for which a different temperature behavior for the HR and LR state would be expected, is therefore at odds with our experiment. In the CBAMR picture,[6] however, the system is expected to be insulating, both in the HR and LR state, and is consistent with our results. The model is based on the assumption that disorder potential fluctuations together with side-wall carrier depletion create small isolated islands in the constriction.

To prove that in our (Ga,Mn)As point contacts Coulomb blockade is at work we investigated samples with additional side-gate electrodes. The nonlinearity of the *I-V* characteristic of device B, plotted in Fig. 3(a), clearly depends on the gate voltage. The corresponding conductance G [Fig. 3(b)], measured in an in-plane field of 0.73 T (Ref. 11) along the [100] direction at $T=0.55$ K, displays pronounced oscillations, indicating Coulomb blockade. These conductance oscillations have an irregular spacing, suggesting that more than one island is formed in the constriction. From the average oscillation period ΔV_g in Fig. 3(b) we estimate a capacitance $C_g\sim 0.55$ aF between gate electrode and islands. For a very rough estimate of the island area we use the charging energy of some meV taken from the *I-V* characteristics. This gives a total capacitance C_Σ of order 10 aF. By approximating the island as a sphere we thus expect a radius of order 10 nm consistent with the constriction size of our device. The pronounced CB diamondlike structure in Fig. 3(c) highlights the role of CB in transport across (Ga,Mn)As point contacts. The anisotropy of the resistance and its dependence on V_g is most clearly seen in Fig. 3(d) where polar plots of R_{sd} are

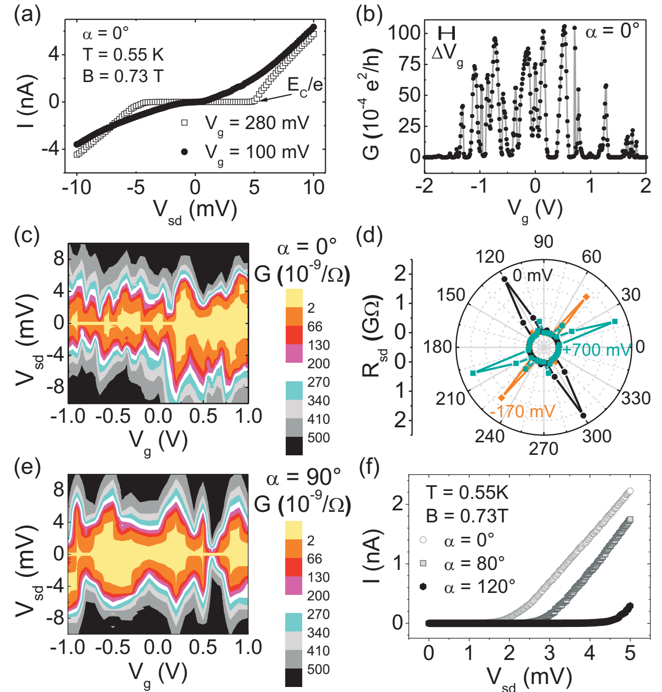

FIG. 3. (Color) (a) *I-V* characteristics of sample B for two different gate voltages showing that the device acts as a transistor. (b) Dependence of the conductance on the gate voltage for $\alpha=0°$ and $V_{sd}=3$ mV. The oscillating behavior is ascribed to a CB transport. ΔV_g stands for the average oscillation period. (c) Color plot of the conductance versus gate and source-drain voltage for 0° resulting in a CB diamondlike structure. (d) Polar plot of R_{sd} for different gate voltages. (e) CB diamondlike structure for $\alpha=90°$ illustrating that the pattern changes for different magnetization directions. (f) *I-V* characteristics for different magnetization directions. Gate voltage and magnetization are independent parameters which allow to tune the conductance. All measurements were carried out at $B=0.73$ T and $T=0.55$ K.

shown for three gate voltages. With different gate voltage the direction of B and hence of the magnetization where the largest resistance is observed changes. Hence, both, gate voltage and magnetization [see Fig. 3(f)] are independent parameters which allow us to tune the conductance through ferromagnetic (Ga,Mn)As islands. It is therefore not astonishing that the CB diamond pattern changes for different magnetization directions. This behavior is illustrated in Fig. 3(e) where, in comparison to (c), the magnetization is rotated by 90°. The underlying physics has been described by Wunderlich *et al.*[6] within the CBAMR model and is due to (different) changes in the chemical potential inside and outside of conducting (Ga,Mn)As islands. Due to the strong spin-orbit coupling in (Ga,Mn)As the chemical potential in the island depends on both the gate voltage and the magnetization direction. These effects might be enhanced by the magneto-Coulomb effect.[12] The different resistance anisotropy for devices A and B at $V_g=0$ [see Figs. 1(b) and 3(d)] can be explained by a different electrostatic environment in the vicinity of the constriction due to thermal cycling.[13] We note that gate-dependent conductance oscillations and CB diamondlike structures were observed in several samples fabricated from the same 20-nm-thick wafer. Whether such

effects can be observed depends not only on the lithographically defined geometry of the constriction but also on the used (Ga,Mn)As bulk material. While in 5 nm thin (Ga,Mn)As films constrictions of 30–40 nm width are sufficient to observe the huge magnetoresistance effects[2,6] we need to fabricate smaller constrictions of ~20 nm width to obtain large effects in our 20-nm-thick material. However, even in a low-doped 50-nm-thick material we successfully fabricated samples showing huge MR effects.[3] Thus, the manganese content and therefore the carrier concentration and sheet resistance of the bulk material are crucial for fabricating (Ga,Mn)As single-electron transistors. This is consistent with the picture that side depletion and the formation of conducting islands separated by insulating (Ga,Mn)As regions play a decisive role for the occurrence of the huge magnetoresistance effects (see below).

V. MODELING THE CONSTRICTED REGION AS A GRANULAR METAL SYSTEM AND ESTIMATION OF THE NUMBER OF ISLANDS

As a result of the gate measurements we conclude that more than one conducting island is located within the nanoconstriction. To elucidate the transport mechanism further we studied the temperature and bias-voltage dependence of the conductance G across the constriction. Corresponding data are shown in Fig. 4 for both, HR and LR state.[14] While in Figs. 4(a) and 4(b) the conductance is plotted as a function of $1/\sqrt{T}$, Figs. 4(e) and 4(f) display G as a function of T for different source-drain voltages V_{sd}. The conductance shows a strong bias dependence [see also Figs. 4(c) and 4(d)]. Such behavior is expected once Coulomb blockade is involved in the transport process. As our system is reminiscent of a granular metal film—metal grains separated by insulating shells—which have been investigated intensively in the past (see, e.g., Ref. 15 and references therein)—we resorted to a corresponding model. We went back to the model of Abeles *et al.*[15] and applied it to our system. Due to the surface depletion in the nanoconstriction we assume that metallic spots of (Ga,Mn)As are separated from each other by thin insulating regions, thus justifying the granular metal assumption. As shown below the modeled bias and temperature dependence of the conductance fits perfectly the experimentally observed data. The granular model distinguishes two regimes reflecting the interplay of the involved energy scales: the thermal energy k_BT, the charging energy $E_C=e^2/2C_\Sigma$, and the energy associated with the average voltage drop across one island $e\Delta V=eV_{sd}/N$. Here, N indicates the number of islands where the voltage drop occurs. For low electric fields where $e\Delta V$ is much smaller than k_BT the model is mainly based on charge-carrier generation by thermal activation and predicts $G(T)=G_0\exp\{-2(C/\sqrt{k_BT})\}$. Here, C is a constant proportional to the charging energy. However, our experiments are clearly not in this low-field regime since the data do not follow the $\ln G\propto T^{-1/2}$ dependence over the entire temperature range shown in Figs. 4(a) and 4(b), both for the HR and LR state. This is consistent with a simple estimate: for our highest temperature of 0.8 K corresponding to $k_BT/e\sim 0.07$ mV and lowest applied bias voltage, $V_{sd}=2.1$ mV, the low-field regime requires that the number of islands N is much larger than 30. Considering the dimensions of our constriction this is highly unlikely. Thus, we have to examine the high-field regime ($e\Delta V\geq k_BT$), where field-induced tunneling becomes important and increases the carrier density. In this case the conductance is given by[15]

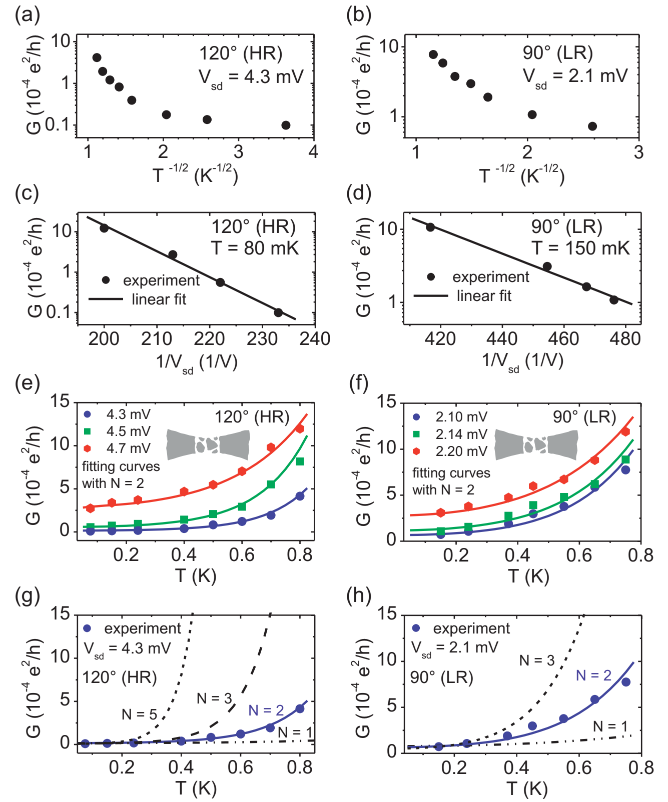

FIG. 4. (Color) [(a)–(b)] log G versus $T^{-1/2}$ plot in a HR and LR state realized by applying a B field of 730 mT along 120° and 90°, respectively, showing that our experiments are not consistent with the low-field regime of the model for granular metal films. [(c)–(d)] Voltage dependence of G showing a good agreement with the model for the high-field regime. From the linear fit we obtain $\ln[G_\infty(HR)/10^{-4}e^2/h]=32\pm 2$, $V_0=(0.15\pm 0.01)$ V for $\alpha=120°$ (HR) and $\ln[G_\infty(LR)/10^{-4}e^2/h]=18\pm 2$, $V_0=(0.038\pm 0.003)$ V for $\alpha=90°$. [(e)–(f)] Experimental data and numerical fits for the temperature dependence of G for different V_{sd} for HR and LR state, respectively. N is the fitting parameter and indicates the number of islands which are schematically illustrated in the inset. The sensitivity of N is demonstrated in (g) and (h).

$$G(T,V_{sd}) = G_\infty \exp\left(-\frac{V_0}{V_{sd}}\right)\int_{-V_0/V_{sd}}^{\infty} dZ \times \frac{Z\exp(-Z)}{1-\exp\left\{-\frac{Ze(V_{sd}/N)}{\left(Z+\frac{V_0}{V_{sd}}\right)k_BT}\right\}} \quad (1)$$

with the electron charge e and the constant V_0 depending on the charging energy. Z is the integration variable. In the limiting case of zero temperature the conductance is given by

$$G(V_{sd}) = G_{\infty} \exp(-V_0/V_{sd}). \quad (2)$$

Hence, plotting ln G versus $1/V_{sd}$ at the lowest temperature allows to estimate both G_{∞} and V_0 directly from experiment. The corresponding data are shown for the HR and LR state in Figs. 4(c) and 4(d), respectively.[16] The only undetermined parameter in Eq. (1) is the number of islands N which we use as the only free fit parameter. The experimental data at temperatures below 1 K, plotted for different bias voltages and for HR and LR states in Figs. 4(e) and 4(f), respectively, can be very well fitted by using $N=2$. Equation (1) describes the temperature dependence for all three traces correctly, both for HR and LR state, using within the error margins the same values for G_{∞} and V_0 given in the caption of Fig. 4. The high sensitivity of the fits with respect to the number of islands is demonstrated in Figs. 4(g) and 4(h). Assuming that the constriction contains two islands and using the previously estimated island size of 20 nm diameter suggests an individual island diameter of order 10 nm. The granular metal model, though at the fringe of applicability given the low N value, describes surprisingly well the bias and temperature dependence of the conductance. This provides further evidence that Coulomb blockade plays a prominent role in transport through (Ga,Mn)As nanoconstrictions and is responsible for the huge magnetoresistance effects observed.

VI. SUMMARY

We revisited the phenomenon of huge magnetoresistances measured across nanoconstrictions in ferromagnetic (Ga,Mn)As films. Our data show that large magnetoresistance effects occur only if the (Ga,Mn)As in the constriction is insulating. Gate-voltage-dependent measurements clearly show that Coulomb blockade plays a decisive role in electrical transport across nanoconstrictions. In addition to the gate voltage, the magnetization direction of the island(s) provides another means to tune the conductance. The interplay of the relevant energy scales of the system, Coulomb charging energy $e^2/2C$, thermal energy k_BT, and the applied bias eV_{sd} are responsible for the pronounced dependence of the resistance on bias voltage, gate voltage, and temperature. A model, originally derived for granular metallic systems, allows to describe the bias and temperature dependence of the nanoconstriction's conductance quantitatively. Fitting the experimental data reveals that only a small number of islands is involved in transport.

ACKNOWLEDGMENT

We acknowledge support from the Deutsche Forschungsgemeinschaft (DFG) via SFB 689.

[1] C. Rüster, T. Borzenko, C. Gould, G. Schmidt, L. W. Molenkamp, X. Liu, T. J. Wojtowicz, J. K. Furdyna, Z. G. Yu, and M. E. Flatté, Phys. Rev. Lett. **91**, 216602 (2003).

[2] A. D. Giddings, M. N. Khalid, T. Jungwirth, J. Wunderlich, S. Yasin, R. P. Campion, K. W. Edmonds, J. Sinova, K. Ito, K. Y. Wang, D. Williams, B. L. Gallagher, and C. T. Foxon, Phys. Rev. Lett. **94**, 127202 (2005).

[3] M. Schlapps, M. Doeppe, K. Wagner, M. Reinwald, W. Wegscheider, and D. Weiss, Physica Status Solidi A **203**, 3597 (2006).

[4] M. Ciorga, M. Schlapps, A. Einwanger, S. Geißler, J. Sadowski, W. Wegscheider, and D. Weiss, New J. Phys. **9**, 351 (2007).

[5] K. Pappert, S. Hümpfner, C. Gould, J. Wenisch, K. Brunner, G. Schmidt, and L. W. Molenkamp, Nat. Phys. **3**, 573 (2007).

[6] J. Wunderlich, T. Jungwirth, B. Kaestner, A. C. Irvine, A. B. Shick, N. Stone, K. Y. Wang, U. Rana, A. D. Giddings, C. T. Foxon, R. P. Campion, D. A. Williams, and B. L. Gallagher, Phys. Rev. Lett. **97**, 077201 (2006).

[7] C. Gould, C. Rüster, T. Jungwirth, E. Girgis, G. M. Schott, R. Giraud, K. Brunner, G. Schmidt, and L. W. Molenkamp, Phys. Rev. Lett. **93**, 117203 (2004).

[8] K. Pappert, M. J. Schmidt, S. Hümpfner, C. Rüster, G. M. Schott, K. Brunner, C. Gould, G. Schmidt, and L. W. Molenkamp, Phys. Rev. Lett. **97**, 186402 (2006).

[9] V. Novák, K. Olejník, J. Wunderlich, M. Cukr, K. Výborný, A. W. Rushforth, K. W. Edmonds, R. P. Campion, B. L. Gallagher, J. Sinova, and T. Jungwirth, Phys. Rev. Lett. **101**, 077201 (2008).

[10] J. Wenisch, C. Gould, L. Ebel, J. Storz, K. Pappert, M. J. Schmidt, C. Kumpf, G. Schmidt, K. Brunner, and L. W. Molenkamp, Phys. Rev. Lett. **99**, 077201 (2007).

[11] The B field that forces the magnetizations into the field direction is larger for lower temperatures.

[12] K. Ono, H. Shimada, and Y. Ootuka, J. Phys. Soc. Jpn. **66**, 1261 (1997).

[13] A. D. Giddings, O. N. Makarovsky, M. N. Khalid, S. Yasin, K. W. Edmonds, R. P. Campion, J. Wunderlich, T. Jungwirth, D. A. Williams, B. L. Gallagher, and C. T. Foxon, New J. Phys. **10**, 085004 (2008).

[14] The HR and LR state was realized, respectively, by applying a sufficiently high magnetic field to align the magnetization into a direction where, at $V_g=0$, a high and low resistance was observed. Here, along 120° and 90°, respectively.

[15] B. Abeles, Ping Sheng, M. D. Coutts, and Y. Arie, Adv. Phys. **24**, 407 (1975).

[16] Only a limited V_{sd} range is accessible for fitting: for smaller voltages the conductance gets immeasurable low while for higher voltages the temperature dependence vanishes.